How do Velocity Structure Functions Trace Turbulence in Simulated Molecular Clouds?

R.-A. Chira[1], J. C. Ibáñez-Mejía[2,3], M.-M. Mac Low[4,5], and Th. Henning[1]

[1] Max-Planck-Institut für Astronomie, Königstuhl 17, 69117 Heidelberg, Germany
e-mail: roxana-adela.chira@alumni.uni-heidelberg.de
[2] I. Physikalisches Institut, Universität zu Köln, Zülpicher Straße 77, 50937 Köln, Germany
e-mail: ibanez@ph1.uni-koeln.de
[3] Max-Planck-Institut für Extraterrestrische Physik, Giessenbachstrasse 1, 85748 Garching, Germany
[4] Dept. of Astrophysics, American Museum of Natural History, 79th St. at Central Park West, New York, NY 10024, USA
e-mail: mordecai@amnh.org
[5] Zentrum für Astronomie, Institut für Theoretische Astrophysik, Universität Heidelberg, Albert-Ueberle-Str. 2, 69120 Heidelberg, Germany

draft of April 24, 2018

Abstract

Context. For a long time it has been argued that turbulence is an important requirement for the formation and evolution of molecular clouds (MCs). It is supposed to be the dominant process that stabilises MCs against gravitational collapse and supports the formation of hierarchical sub-structures. Yet, little is still known about the sources of turbulence that dominates the velocity structure on scales of entire MCs.

Aims. We investigate the time evolution of turbulence within modelled clouds. In particular, we focus on the following questions: What dominantly drives turbulent motions within MCs? And is there a method that traces these dominant modes based on both simulated and observational data?

Methods. We follow the gas motions within three MCs that have formed self-consistently within kiloparsec-scale numerical simulations of the interstellar medium (ISM) performed with the FLASH adaptive mesh refinement magnetohydrodynamic code. The simulated ISM evolves under the influence of different physical processes, i.e. self-gravity, magnetic fields, supernovae-driven turbulence, and radiative heating and cooling. We express the distribution of turbulent power in terms of velocity structure functions (VSFs) and compare the time evolution of obtained parameters with predicted values.

Results. We demonstrate that the scaling exponent of VSFs and the priciple of self-similarity are sensitive tools that trace the dominant sources of turbulence driving in both simulated and observational data. When gravity dominates the dynamics of the gas, the scaling exponents decline while the self-similarity parameters are constant. When the gas is interacting with shocks or strong winds the exponents increase while the self-similarity parameters decline. The effect of such interactions, however, lasts only for short periods of time (< 0.6 Myr) in our simulations. These trends are generally robust against the influence of projection, level of Jeans refinement and density-weighting. Yet, the detailed evolution may vary significantly. Only varying the density threshold, that defines which regions are considered in the analysis, has a significant influence on the VSFs.

Conclusions. We conclude that the VSF is a well placed and stable method for examining the composition, structure and evolution of turbulence within the MCs. Yet, it is essential to clearly define the underlying conditions and assumptions of the analysis in order to clarify which part of the ISM is studied and to make the results comparable to analogue studies. In our case, we find clear indicators of how the VSF reacts to the dynamics in the simulated clouds. The turbulence in the clouds is dominantly driven by contraction, as a reaction to the on-set of self-gravity within the simulations. Occasionally, SN shocks disturb the dynamics within the clouds and inject new kinetic energy on large scales into the systems. Yet, the effect lasts only for a short period of time before gravity dominates the energy cascade again.

Key words. keywords

1. Introduction

It has long been know that star formation preferentially occurs in molecular clouds (MCs). Yet the exact set-up that leads to the on-set of star-forming activities is still not completely understood. It is clear that gravity is the major factor as it drives collapse motions and operates on all scales. However, one needs additional processes that stabilise the gas in order to explain the long life times of MCs, low star formation efficiencies and the formation of (filamentary) sub-structures observed in MCs. Although there are many processes that act on the different scales of MCs, turbulence is traditionally supposed to be the best candidate for this task.

In literature, turbulence has an ambiguous role in the context of star formation. In most of the cases, turbulence is expected to stabilise molecular clouds on large scales (Fleck 1980; McKee & Zweibel 1992; Mac Low 2003), while feedback processes and shear motions heavily destabilise or even disrupt cloud-like structures, offering a formation scenario for large filaments (Tan et al. 2013; Miyamoto et al. 2014). However, it is not entirely clear whether there are particular mechanisms that dominantly drive the turbulence with MCs, although all of them are supposed to show different imprints in the observables. For example, turbulence that is driven by large-scale velocity dispersions during global collapse (Ballesteros-Paredes et al. 2011a,b;

Hartmann et al. 2012) produces P-Cygni lines. Despite that such lines are normally not observed, this process cannot explain the long lifetimes of giant molecular clouds. Internal feedback, contrary, seems more promising as it drives turbulence outwards (Dekel & Krumholz 2013; Krumholz et al. 2014). Observations, though, demonstrate that the required driving sources need to act on scales of entire clouds; which typical feedback processes cannot achieve (Brunt et al. 2009; Brunt & Heyer 2013; Heyer & Brunt 2004).

There have also been many theoretical studies that have examined the nature and origin of turbulence within the phases of the ISM (Mac Low & Klessen 2004, and references within). The most established work has been conducted by Kolmogorov (1941) who investigated fully developed, incompressible turbulence that is driven on scales larger than the object of interest. In the scope of this paper this object is a single molecular cloud. The underlying assumptions of Kolmogorov's describe the very special scenario of a divergence-free velocity field. This is not necessarily the case in a MC, yet analytical studies without these assumptions are still rare, but exist. She & Lévêque (1994) and Boldyrev (2002), for example, generalise and extend the predicted scaling of the decay of turbulence to supersonic turbulence. Galtier & Banerjee (2011) and Banerjee & Galtier (2013) provide an analytic description of the scaling of mass-weighted structure functions.

— continue proof-reading —

In this paper, we examine three molecular clouds that formed self-similarity in the simulations by Ibáñez-Mejía et al. (2016, Paper I, hereafter) and study the evolution of turbulence as traced by the gas within the model clouds. The key questions we answer are the following: What dominates the turbulence within the simulated molecular clouds? Is there a method that can trace the dominant modes reliably, also in observational studies?

In Sect. 2, we introduce the model clouds in the context of the underlying simulations, as well as the theoretical basics of velocity structures functions. Sect. 3 demonstrates that velocity structure functions are a useful tool to characterise the dominant driven source of turbulence in molecular clouds and can be applied on both simulated and observed data. Furthermore, we also discuss the influences of utilising one-dimensional velocity measurements, different Jeans refinement levels, density thresholds and density weighting have on the applicability of velocity structure functions and the results obtained with them. We summarise our findings and conclusions in Sect. 5.

2. Methods

2.1. Cloud models

[general comment: In this sub-section I basically copied the descriptions we have used in the previous paper. I am not sure whether the summary given here in to short as I also wanted to provide a summary of the work we have done with the data already. I would appreciate what you think about the structure of this subsection.]

The analysis in this paper is based on a sample of clouds found within the 3D magnetohydrodynamics (MHD), AMR FLASH code (Fryxell et al. 2000) simulations by Ibáñez-Mejía et al. (2016). Ibáñez-Mejía et al. (2016, 2017, hereafter Paper I and Paper II, respectively) and Chira et al. (2017, hereafter Paper III) describe the simulations and the clouds in details. For the context of this paper, we summarise the most important properties.

The entire 3D MHD AMR simulations model a multi-phase, turbulent interstellar medium (ISM) of a disk galaxy, where dense structures form self-consistently in turbulent, convergent flows (Paper I). The simulations include gravity (stellar potential and dark matter halo; after 250 Myr also self-gravity), supernova-driven turbulence, photoelectric heating and radiative cooling, as well as magnetic fields. The three clouds we analyse in this paper are small $(40 \text{ pc})^3$ subregions of the entire $1 \times 1 \times 40 \text{ kpc}^3$ volume. The authors of Paper II have re-simulated the clouds with an effective spatial resolution of $\Delta x_{\min} = 0.1$ pc when mapped onto a $400 \times 400 \times 400$ grid cells containing cube, respectively. Objects with the clouds are fully resolved if their local Jeans length $\lambda_J > 4 \Delta x_{\min}$, corresponding to a maximum resolved density at 10 K of $8 \times 10^3 \text{ cm}^{-3}$ (e.g. Paper II, Eq. 15). This means that we can trace fragmentation down to 0.4 pc, but cannot fully resolve objects that form at smaller scales. The clouds have total masses on the order of 3×10^3, 4×10^3, and $8 \times 10^3 \text{ M}_\odot$ (hereafter denoted models M3, M4, and M8).

This set-up opens opportunities for many different kind of studies. The authors of Paper II have described the properties of all three clouds in detail, as well as followed the time evolution of those properties. In particular focus, the authors have investigated typical observables, such as mass, velocity dispersion and Mach number, in context of molecular cloud formation within spiral galaxies. In Paper III we have studied the properties and time evolution, as well as the fragmentation behaviour of filaments that condense within the model clouds.

In this paper, we focus on the driving sources of turbulence within the modelled molecular clouds and which signatures they print on observables, such as the velocity structure functions.

2.2. Velocity Structure Functions

We probe the power distribution of turbulence throughout the entire modelled molecular clouds by using the so-called velocity structure function (VSF). The VSF is a two-point correlation function that measures the mean velocity difference, $\Delta v = v(x + \ell) - v(x)$, between two grid cells x and $x + \ell$ (with ℓ being a direction vector pointing from the first to the second cell of the grid), to the pth order as function of lag distance, $\ell = |\ell|$, between the correlated points. Thereby, the VSF estimates the occurrence of symmetric motions (e.g., rotation, collapse, outflows), as well as rare events of random turbulent flows in velocity patterns that become more prominent the higher p is (Heyer & Brunt 2004). For data on an Eulerian grid, such as ours, the density weighted definition of the VSF, S_p, is given by

$$S_p(\ell) = \frac{\langle \rho(x)\rho(x + \ell) |\Delta v|^p \rangle}{\langle \rho(x)\rho(x + \ell) \rangle}, \quad (1)$$

(Padoan et al. 2016, and references within).

Each order of VSF has a physical meaning. For example, S_1 is correlated to the mean relative velocities between cells, reflecting the modes created by different gas flows. S_2 is proportionally to the kinetic energy, making it a good probe of how the turbulent energy is transferred across different scales.

If the turbulence is fully developed the VSF is supposed to be well-described by a power-law relation (Kolmogorov 1941; She & Lévêque 1994; Boldyrev 2002):

$$S_p(\ell) \propto \ell^{\zeta(p)}. \quad (2)$$

The scaling exponent of that power-law relation, ζ, therefore, not only depends on the order of the VSF, but is also strongly influ-

enced by the properties and composition of the underlying turbulence, like compressibility or Mach number. Many studies on VSFs distinguish between longitudinal and transverse velocity components, or compressible and solenoidal gas flow components since those are expected to behave differently, especially towards larger lag distances (Gotoh et al. 2002; Schmidt et al. 2008; Benzi et al. 2010). However, the differences are mostly negligible on the scales we focus on. This and the fact that those components are observationally very hard differentiable, are the reasons why we analyse all components in a common sample.

There are a few theoretical studies that predict values of $\zeta(p)$ depending on the nature of turbulence. For example, Kolmogorov (1941) predicts the third-order exponent, $\zeta(3)$, to be exactly 1 for an incompressible, transonic flow. This results in the commonly known prediction that the kinetic energy decays with $E_k(k) \propto k^{-\frac{5}{3}}$, with $k = \frac{2\pi}{\ell}$ being the wavenumber of the turbulence mode.

For a supersonic flow, however, it is always supposed to be greater or equal to unity. Based on Kolmogorov's work, She & Lévêque (1994) and Boldyrev (2002) have extended and generalised the analysis and predict the following. For an incompressible filamentary flow She & Lévêque (1994) predict that the VSFs scale with,

$$\zeta_{\text{She}}(p) = \frac{p}{9} + 2\left[1 - \left(\frac{2}{3}\right)^{\frac{p}{3}}\right] = Z_{\text{She}}(p), \qquad (3)$$

while supersonic flows with sheet-like geometry are supposed to scale with (Boldyrev 2002),

$$\zeta_{\text{Boldyrev}}(p) = \frac{p}{9} + 1 - \left(\frac{1}{3}\right)^{\frac{p}{3}} = Z_{\text{Boldyrev}}(p). \qquad (4)$$

Benzi et al. (1993) have introduced the principle of "extended self-similarity" which propose that there is a fixed relation between the a VSF of pth order and the 3rd VSF, so that the ratio

$$Z(p) = \frac{\zeta(p)}{\zeta(3)} \qquad (5)$$

is constant over all lag scales. Since the mentioned predictions of $\zeta(p)$ are normalised in a way that $\zeta(3) = 1$ Eq. (3) and (4) also provide the predictions for $Z(p)$, respectively.

For the discussion below, we measure ζ by fitting a power-law, given by

$$\log_{10}\left[S_p(\ell)\right] = \log_{10}(A) + \zeta \log_{10}(\ell), \qquad (6)$$

with A being the scaling factor of the power-law to the simulated measurements. For the calculations, we only take those cells with a minimal number density of $100\ \text{cm}^{-3}$ into account as this threshold defines the volume of the clouds. For reducing the computational effort we divide the scale of 3D lag distances, ℓ, into 40 equidistantly separated bins ranging from 0.1 to 30 pc. This means that the measurements at the given lag interval ℓ_i we will show below base on the data with lag distances $\ell_{i-1} < \ell \leq \ell_i$.

3. Results

In this section, we present our results on how velocity structure functions (VSFs) reflect the distribution of turbulent power within molecular clouds. Fig. 1 shows three examples of VSFs, namely (a) M4 $t = 1.2$ Myr, after self-gravity has been activated in the simulations, (b) M3 at $t = 3.5$ Myr, and (c) M3 at

$t = 4.0$ Myr. Thereby, the solid lines in the examples illustrate the fitted power-law relations as given in Eq. (6).

All plots illustrate the VSFs of the orders $p = 1$–3 that are computed based on the simulation data. The examples demonstrate that, in general, the measured VSFs cannot be described by a single power-law relation over the entire range of ℓ. Rather they are composed of roughly three different regimes: one at small scales with $\ell \lesssim 3$ pc, a second one within 3 pc $\lesssim \ell \lesssim 10$–15 pc, and the last one at large scales with $\ell > 15$ pc. Therefore, only the small and intermediate ranges may be described by a common power-law relation. On larger scales, one observes a local minimum before the VSFs either increase or remain constant. The location of the minimum, thereby, coincides with the equivalent radius of the cloud, meaning the radius a cloud of given mass would have if it would be a sphere. Thus, in this context the VSF is an accurate tool to measure the size of a molecular cloud. On smaller scales, which correspond to individual clumps and cores, one sees significant differences.

Fig. 2a plots the time evolution of ζ obtained for all three clouds. The figure shows several interesting features. First, initially all calculated values of ζ are above the predicted values (see Eqs. (3) and (4)). This means that the turbulence within the clouds is highly supersonic before the gas begins to react to the activation of self-gravity. Second, all ζ decrease with time as the clouds gravitationally collapse. Therefore, the gas transfers the turbulent power from large to small scales. This process accelerates the relative motions between cells on all scales and causes a flat or even inverted profile in the VSF. Third, occasionally one observes bumps and dips in all orders of VSFs (e.g., M3 or M8 around $t = 1.7$ Myr). These features only last for short periods of time (up to 0.6 Myr), but set in quasi-instantly and represent a complete relocation of the turbulent power on all scales.

Yet, M8 seems to develop differently. At the time the SN, occurring at $t = 0.8$ Myr, hits the cloud the values of ζ do not rise, as they have done within the other two clouds, but instead they drop. After the shock all scaling exponents grow to levels that are slightly above the pre-shock values, before they slowly decrease again.

Fig. 3a shows the time evolution of the scaling of the pth order VSF relative to the 3rd order VSF scaling, $Z(p) = \zeta(p)/\zeta(3)$, based on the model clouds. One sees that most of the time the measured values of $Z(p)$ are in agreement or at least closely approaching the predicted values.

The peaks in the Z (for example, in M4 at $t = 4.1$ Myr) occur at the times when the scaling exponents of the VSFs, ζ, reach values close or below 0. The decrease in Z (for example, in M3 around $t = 1.8$ Myr), on the other hand, occur when SN shocks hit and heavily impact the clouds.

In the following of this section, we will present how VSFs react to variety of setups that are typically assumed in comparable studies. We will compare the findings with the results we have obtained with our original setup. In Sect. 4, we will discuss and interpret these results in more details.

3.1. Comparison to Line-of-Sight Velocities

So far, we have seen how the VSF behaves and evolves within the clouds. By doing so, we derived the relative velocities based on the 3D velocity vectors that we read out from the simulations. Yet, this method is rather not applicable for many other studies. It is, on the one hand, computational expensive or, on the other hand, not possible as observations generally only provide the velocity component along the line-of-sight (los). Thus, in this subsection we investigate how VSFs derived from 1D relative

Figure 1: Examples of velocity structure functions as function of the lag scale, ℓ, and order, p. The dots (connected by dashed lines) illustrate the measured values based on the simulation data. The solid lines represent the power-law relations fitted to the respective structure function.

velocities compare to the 3D VSFs presented before. Thereby, we define the 1D VSF as follows:

$$S_p^{1D}(\ell) = \frac{\langle \rho(\boldsymbol{x})\rho(\boldsymbol{x}+\boldsymbol{\ell})\,|\Delta\boldsymbol{v}\cdot\boldsymbol{e}_i|^p\rangle}{\langle\rho(\boldsymbol{x})\rho(\boldsymbol{x}+\boldsymbol{\ell})\rangle}, \qquad (7)$$

with $\boldsymbol{e}_i$ representing the unit vector along the i = x-, y-, or z-axis. Figs. 2b and 3b show measured ζ and Z, respectively, derived based on Eq. (7). We see that in most of the cases the 1D and 3D VSFs agree well with each other. Yet, there are cases in which the 1D VSF evolves temporarily or completely differently than the 3D VSF. For example, the 1D VSF along the x-axis in M3 initially behaves like the corresponding 3D VSF, if though with lower absolute values of ζ (or higher values of Z). However, within t = 2.5–3.8 Myr the samples diverge. While the 3D based ζ cease further and switch signs, the ζ based on the 1D VSF along the x-axis show a local maximum before converging with the 3D ζ again.

3.2. The Effect of Jeans Length Refinement

The results we have discussed so far are based on simulation data as they have been presented in Paper I and Paper II. Due to the huge computational expense the variety of physical and numerical processes (fluid dynamics, adaptive mesh refinement, supernovae, magnetic fields, radiative heating and cooling, and many more) within those simulations, though, have also demanded some compromises.

One of these compromises has been the Jeans refinement criterion that is part of the AMR mechanisms. The authors have resolved local Jeans lengths by only four cells ($\lambda_J = 4\Delta x$). This is the minimal requirement for modelling self-gravitating gas in order to avoid artificial fragmentation (Truelove et al. 1998). Other studies, for example by Turk et al. (2012), yet have shown that a significant higher refinement is needed to reliably resolve turbulent structures and flows on scales of individual cells.

In the appendix of Paper II, the authors examine the effect the number of cells used for the Jeans refinement has on the measured kinetic energy. For this, they have rerun the simulations of M3 twice; once with a refinement of eight cells per Jeans length ($\lambda_J = 8\Delta x$) for the first 3 Myr after self-gravity was activated, and once with 32 cells per Jeans length ($\lambda_J = 32\Delta x$) for the first megayear of the cloud's evolution. The authors show that the

$\lambda_J = 32\Delta x$ simulations smoothly reveal the energy power spectrum on all scales already after this first megayear. The other two setups also do this. However, they need more time to overcome the resonances in the respective power spectra that originate from the previous resolution steps. This is why one can only fully reliably trust the findings in this paper after the clouds have evolved for approximately 1.5 Myr (see also Ibáñez-Mejía et al. 2017; Seifried et al. 2017).

More importantly, though, Paper II have calculated the difference in the cloud's total kinetic energy as function of time and refinement level. They found that the $\lambda_J = 4\Delta x$ simulations miss a significant amount of kinetic energy, namely up to 13% compared to $\lambda_J = 8\Delta x$ and 33% compared to $\lambda_J = 32\Delta x$. However, they also observed that these differences peak around t = 0.5 Myr and decrease afterwards again, as the $\lambda_J = 4\Delta x$ and $\lambda_J = 8\Delta x$ simulations adjust to the new refinement levels. This, of course, means that the results we have derived from the $\lambda_J = 4\Delta x$ simulations always needs to be evaluated with respect to this lack of energy, although the clouds' dynamics is dominated by gravitational collapse. Yet it also means that the $\lambda_J = 4\Delta x$ data become more reliable the longer the simulations have time to evolve.

In this section, we present how the level of Jeans refinement influences the behaviour of the VSFs. In order to do so, we analyse the data of the $\lambda_J = 8\Delta x$ and $\lambda_J = 32\Delta x$ simulations in the same way as we have done with the $\lambda_J = 4\Delta x$ data: measure the VSFs and analyse the time evolution of ζ and Z. Figs. 2c and 3c plot the measure values of ζ and Z for the $\lambda_J = 8\Delta x$ and $\lambda_J = 32\Delta x$. In Fig. 4 we directly compare the measurements of all refinement levels relative to $\lambda_J = 4\Delta x$.

$\lambda_J = 8\Delta x$ shows the same behaviour as $\lambda_J = 4\Delta x$ previously, with values in both samples being in good agreement as the top panel of Fig. 4 demonstrates. Over the entire observed time span, the measured values of ζ decreases as the VSF become flatter. At the time the SNe interact with the cloud, the VSFs steeply increase forward larger scales, causing values of ζ (Fig. 2c). Compared to $\lambda_J = 4\Delta x$ sample, the peak in ζ is smoother and last longer here, reflecting an impact time span of a bit less than 1 Myr.

This is also observable in Fig. 3c where the sink of Z due to the SN shock lasts longer than it has done in within the $\lambda_J = 4\Delta x$ simulations. Besides this, the time evolution of Z based on the $\lambda_J = 8\Delta x$ simulations is as sensitive to the turbulence-related
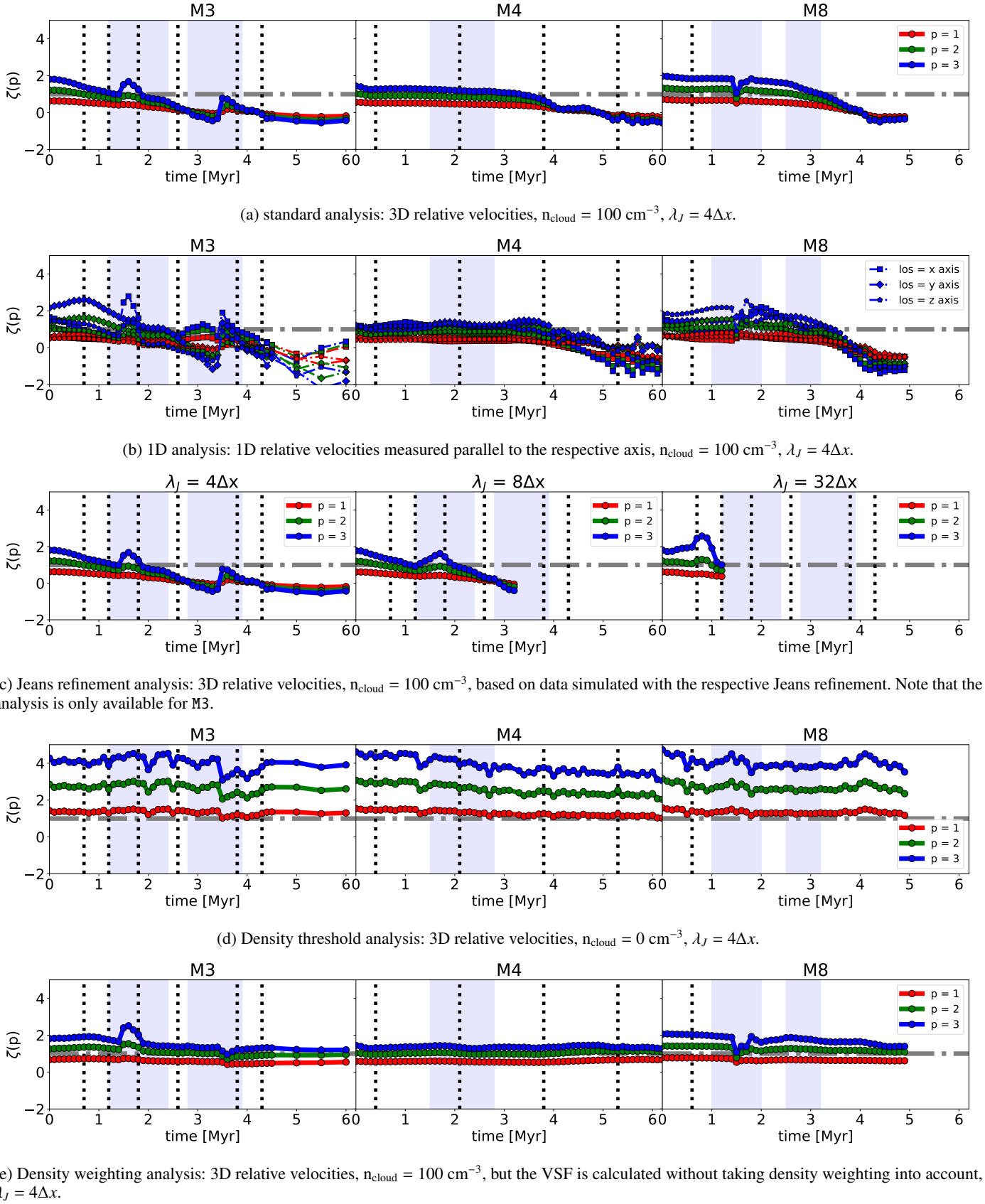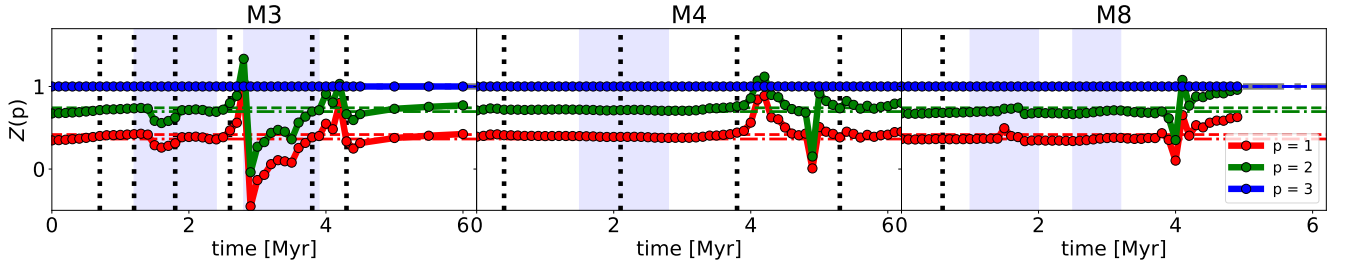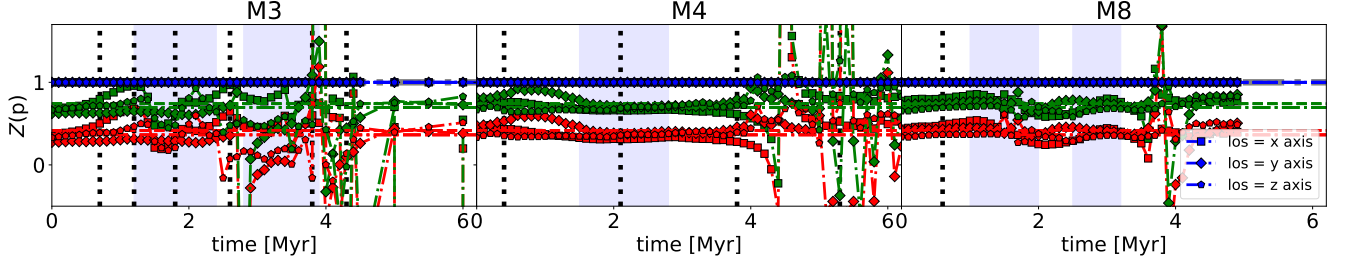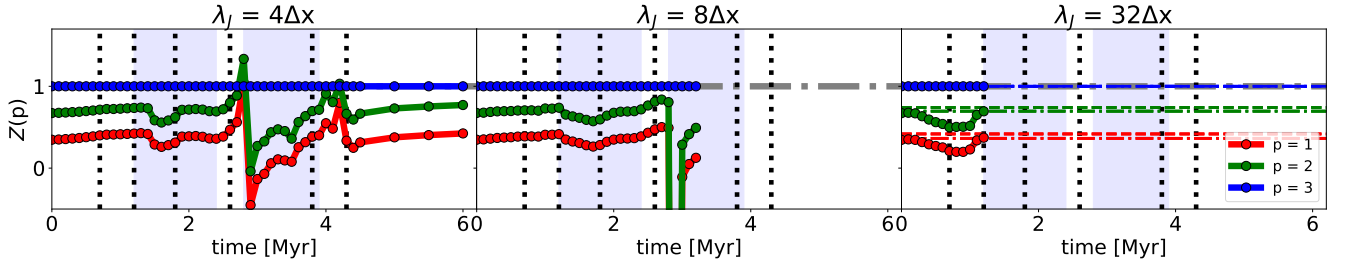
(a) standard analysis: 3D relative velocities, $n_{cloud} = 100\ cm^{-3}$, $\lambda_J = 4\Delta x$.

(b) 1D analysis: 1D relative velocities measured parallel to the respective axis, $n_{cloud} = 100\ cm^{-3}$, $\lambda_J = 4\Delta x$.

(c) Jeans refinement analysis: 3D relative velocities, $n_{cloud} = 100\ cm^{-3}$, based on data simulated with the respective Jeans refinement. Note that the analysis is only available for M3.

(d) Density threshold analysis: 3D relative velocities, $n_{cloud} = 0\ cm^{-3}$, $\lambda_J = 4\Delta x$.

(e) Density weighting analysis: 3D relative velocities, $n_{cloud} = 100\ cm^{-3}$, but the VSF is calculated without taking density weighting into account, $\lambda_J = 4\Delta x$.

Figure 2: Time evolution of scaling exponent ζ of the pth order VSF. The plots (a), (b), (d), and (e) show the measurements for M3 (*left*), M4 (*middle*), and M8 (*right*). Panel (c), though, only illustrate the measurements for M3 with the respective Jeans refinement level. The grey dotted vertical lines point to the times than a SN explodes within the vicinity of the corresponding cloud, while the blue areas indicate the time of enhanced mass accretion onto the clouds.
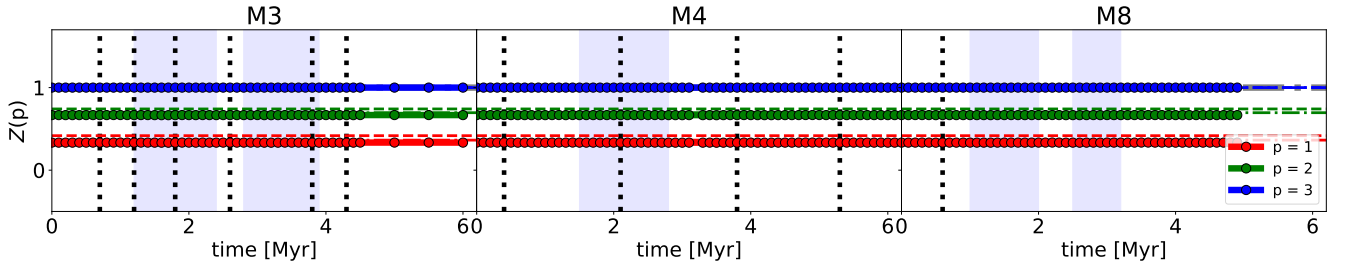
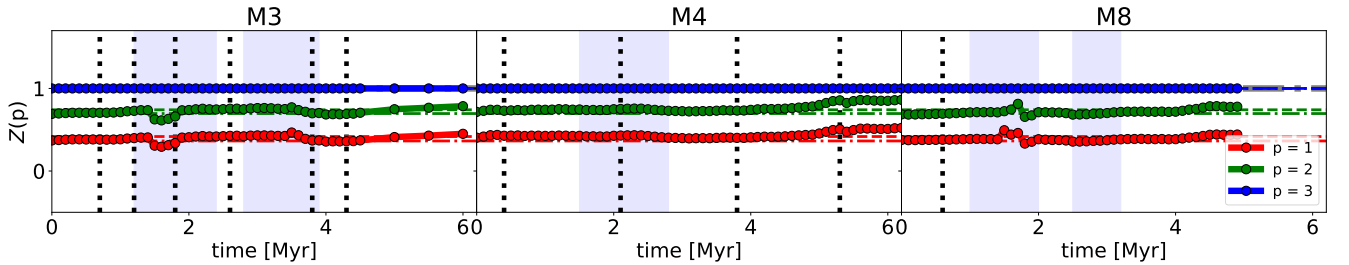(a) standard analysis: 3D relative velocities, $n_{cloud} = 100$ cm^{-3}, $\lambda_J = 4\Delta x$.

(b) 1D analysis: 1D relative velocities measured parallel to the respective axis, $n_{cloud} = 100$ cm^{-3}, $\lambda_J = 4\Delta x$.

(c) Jeans refinement analysis: 3D relative velocities, $n_{cloud} = 100$ cm^{-3}, based on data simulated with the respective Jeans refinement. Note that the analysis is only available for M3.

(d) Density threshold analysis: 3D relative velocities, $n_{cloud} = 0$ cm^{-3}, $\lambda_J = 4\Delta x$.

(e) Density weighting analysis: 3D relative velocities, $n_{cloud} = 100$ cm^{-3}, but the VSF is calculated without taking density weighting into account, $\lambda_J = 4\Delta x$.

Figure 3: Like Fig. 2, but for the measured self-similarity parameter $Z = \zeta(p)/\zeta(3)$ of the pth order VSF. The coloured horizontal lines show the predicted values by She & Lévêque (1994) (dash-dotted lines) and Boldyrev (2002) (dashed lines).

events as it has been for $\lambda_J = 4\Delta x$. The divergence which is produced when gravity has transferred the majority of power to smaller scales occurs at the same time. The depth of the sink is thereby a numerical artefact caused by $\zeta(3)$ being equal or close to 0 at this very time step.

The picture changes when analysing the VSFs based on the $\lambda_J = 32\Delta x$ runs (Figs. 2c, 3c, and 4 *bottom* panel). Here one sees that the measured values of both ζ (Fig. 2c) and Z (Fig. 3c) are similar to those for $\lambda_J = 4\Delta x$ for the first 0.2 Myr. After this short period, though, the evolutions of ζ diverge. While $\zeta(1)$ and $\zeta(2)$ continue to decrease in similar, but lower rates compared to $\lambda_J = 4\Delta x$, $\zeta(3)$ increases until it peaks at $t = 0.8$ Myr, before it falls steeply down again. At $t = 1.2$ Myr, the last time step of this sample, the values of all ζ equal the measurements of $\lambda_J = 4\Delta x$ again (see also Fig. 4). However, since there is no information of how the $\lambda_J = 32\Delta x$ simulations develop further we cannot predict whether this correspondence will continue.

The bottom panel of Fig. 4 illustrates the different evolutions of measured ζ and Z in the two samples of simulations more clearly. One sees that the differences between the simulation samples follow the same pattern for all orders of p. The order of difference, though, increases with the order: While the values for $\zeta(1)$ are still in good agreement, the measured values of $\zeta(2)$ and $\zeta(3)$ for $\lambda_J = 32\Delta x$ are 40% and 100% higher than those measured for $\lambda_J = 4\Delta x$, respectively. Consequently, this causes differences in $Z(p)$ within 30–52% between the simulations.

3.3. The Effect of Density Thresholds

Another assumption that significantly influence the structure and evolution of VSFs is the density threshold we have applied to filter out the cells that are part of the clouds. In this paper, we assume a minimal number density that defines the clouds' volume of $n_{\text{cloud}} = 100$ cm^{-3}. This means that, when focusing on the cloud-only matter, we only consider those cells with number densities $n \geq n_{\text{cloud}}$. We have chosen this threshold as it roughly corresponds to the density when CO becomes detectable.

However, Paper II show that there is usually no harsh jump in density between the ISM and the clouds. Instead, the density increases continuously towards the centres of mass within the clouds. Consequently, introducing a density threshold is a rather artificially, weakly physically motivated distinction between the clouds and the ISM. Observationally, however, introducing a density (or intensity) threshold is unavoidable, be it due to technical limitations (e.g., sensibility of detector) or the nature of the underlying physical processes (for example, excitation rates, or critical density). Therefore, it is important to study to which extend a density threshold influences the VSF and its evolution.

In Figs. 2d and 3d we show our measurements for ζ and Z, respectively, without introducing an density threshold. This means that we now do not only measure the relative velocities between cells that are part of the clouds' volume, but between cells within the entire 400^3 cell cut-outs that contain both the clouds and the ISM. For our calculations we apply the same methods as described in Sect. 2. Yet, in order to reduce the computational effort we have chosen only a randomly positioned subset of cells within the entire cubes. This means that the results shown here are based on 3,200,000 cells (= 5% of the entire 400^3 cube). As the random selection of cells and the clouds make up only a small fraction of the volume within the cubes, this approach makes it more like to pick locations within the modelled ISM, rather than cells within the clouds. Please note, that by doing so we only influence the choice of x in Eq. (1), not

$x + \ell$ as we still compute the relative velocities relative to every other cell at 3D lag distance ℓ within the entire cube.

The figures clearly illustrate that the measurements in the samples without density threshold completely differ from those with the density threshold. Fig. 2d shows that the measured values of ζ are by far higher in the ISM than in the cloud-only sample. Furthermore, although we see a similar decline of ζ in M4 and M8 as the gas contracts under the influence of gravity in the vicinity of the clouds, ζ generally evolve differently here than what we have observed for the cloud-only matter. E.g., the pronounced features that have reflected the interactions between the clouds' mass and shock waves are either not as significantly visible or not present at all. We see a high rate of random fluctuations in the evolution of ζ, as well. That those fluctuations really represent the turbulent nature of the ISM gas and not a super-position of multiple shocks, that are too weak to influence the compact clouds, becomes evident in the evolution of Z (see Fig. 3d). Contrary to all of our other test scenarios, all Z here are constant in time and within all clouds, with values slightly lower than those predicted by She & Lévêque (1994) for filamentary flows.

3.4. The Effect of Density Weighting

As mentioned previously, Eq. (1) represents the definition of the density-weighted VSF. The density weighting is required for this study to account for obtaining smooth density distributions on Eulerian grids from the simulations, instead of using individual Lagrangian test particles (or eddies) as one is actually supposed to. Thus, a natural question to ask is how the two ansatzes compare with each other. There are a few studies that have targeted this question **(ref!!!)**. Yet all of them considered turbulent flows in sterile, homogeneous environments that are not comparable to our clouds. Other studies, like Padoan et al. (2016), use both methods, but not on the same set of data.

In this section, we investigate the influence of density weighting on VSFs. For this, we repeat the analysis, but now using the non-weighted VSF as given by,

$$S_p(\ell) = \langle |\Delta v|^p \rangle = \langle |v(x) - v(x + \ell)|^p \rangle. \tag{8}$$

Figs. 2e and 3e show the measured values of ζ and Z derived from the non-weighted VSFs based on the $\lambda = 4\Delta x$, respectively.

Comparing the weighted and non-weighted samples, we see the following: The non-weighted ζ (Fig. 2e) and Z (Fig. 3e) trace the interactions between the gas of the clouds and the SN shocks in the same way as we have seen it for the density-weighted VSF. In M3 and M8 we also see that the values of ζ decrease as the clouds evolve. The measurements in M4, however, are almost constant over time. In all the cases, the values of ζ never cease below 0.5; a behaviour that clearly differs from what we have observed in the density-weighted VSFs.

For the measured Z values we see a similar behaviour. As before, they are almost constant over time and in good agreement with predicted values. The only derivations we see compared to the previous results are caused by the interactions between the clouds and incoming SN shock fronts, with levels of disturbance that are identical with our measurements using density-weighted VSFs. Yet, the evolution of Zs is smoother here as we do not measure any sign inversion of ζ. This means that we do not have any strong peaks in Z indicating the time when most of the turbulent power is transferred to the small scales.

Fig. 5 summarises the comparison of ζ (*top*) and Z (*bottom*) measured with the density-weighted (*abscissas*) and non-
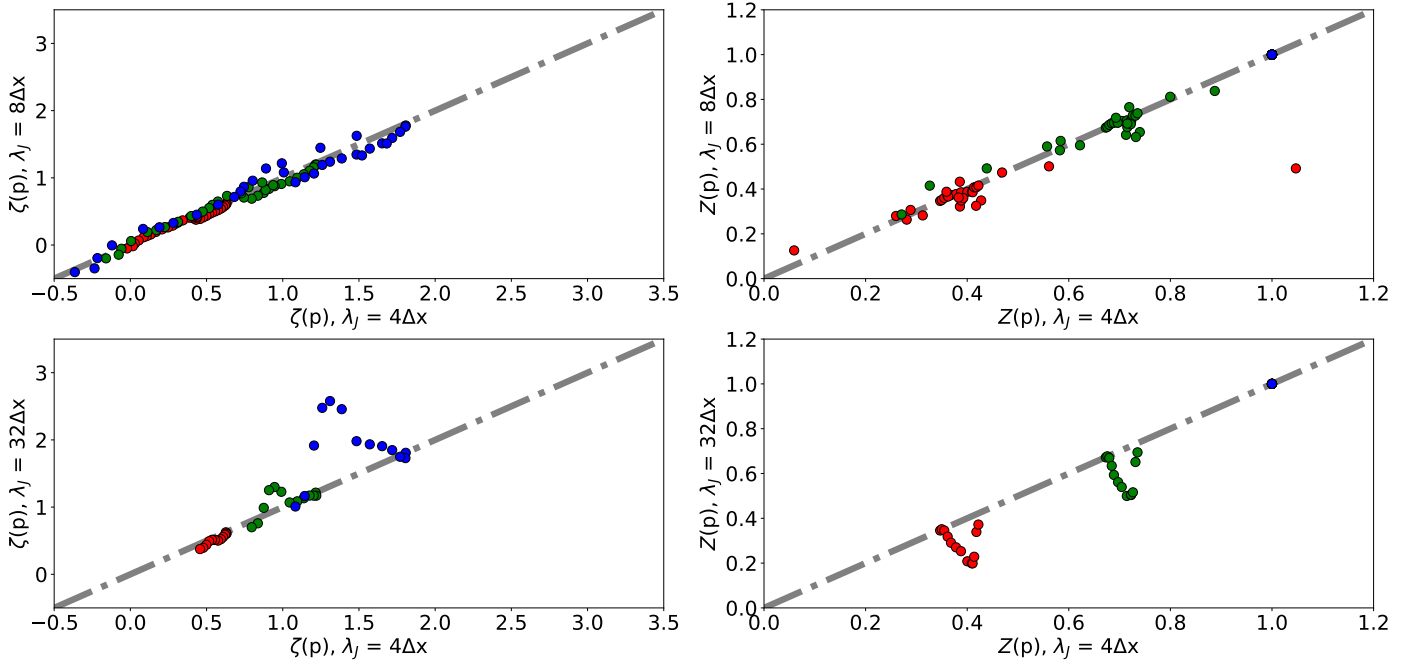
Figure 4: Caption.

weighted VSFs (*ordinates*) for all refinement levels. The figure clearly shows that the measurements only agree well for the highest refinement level with $\lambda = 32\Delta x$. Yet we would need more data point to be sure that this correlation is indeed real. With lower refinement level the measurements correlate less well with each other. However, the differences in the samples appear dominantly when the density-weighted ζ cease below ≈ 0.5, which is the global minimum for the non-weighted ζ. This means that none of the ζ computed in all clouds and refinement levels with the non-weighted VSF is measured to be below 0.5. Thus, we can trace the discrepancies between the scaling exponents of density-weighted and non-weighted VSFs back to the disability of the non-weighted VSFs to follow the transition form large-scale driven to small-scale dominated distributions of turbulent power.

4. Discussion

The examples in Fig. 1 illustrate how the clouds and their VSFs react to different scenarios that affect the turbulent structure of the entire clouds. In Fig. 1a one sees the standard case where turbulence is fully developed, driven on large scales and decays to small scales. This is the dominant case within the first ~1.5 Myr of the simulations. During this interval of time the clouds experience the effect of self-gravity for the first time in their evolution and need to adjust to this new condition. Until this is the case, their VSFs are dominated by the freely cascading turbulence that previously dominated the kinetic structure of the clouds. Furthermore, this implies that we can only reliably examine turbulence within the simulations after 1.5 Myr and carefully need to take this into account in the further discussion (see Ibáñez-Mejía et al. 2017; Seifried et al. 2017).

The other examples represent the clouds at later stages of their evolution when the VSFs are dominated by sources that drive the turbulence within the clouds in a more extreme way. Fig. 1b shows the VSF of M3 at a time when the cloud has just been hit by a supernova (SN) shock front. One clearly sees how the amplitude of the VSFs is increased by one to two orders of

magnitudes compared to the previous example. Especially the power of small scale turbulence ($\ell \lesssim$ few parsecs) is highly amplified as result of the shock, while it reduces the equivalent radius of the cloud. Despite the increase of turbulent power at small scales, there is a great amount of energy injected at large scales, as well. All this results in a steeper scaling of the VSF. However, the effect of SN shocks last for only a short period of time (see below).

The last example, Fig. 1c, demonstrates the imprint of gravitational contraction. Here, the VSF is almost flat, or even slightly increasing towards smaller separation scales. This kind of profile is typical for gas that is self-gravitationally contracting (Boneberg et al. 2015; Burkhart et al. 2015) since gas moves into the inner regions of the cloud, reducing the average lag distances, but not necessarily the relative velocities. The latter may even be accelerated by the infall. As a consequence, large amounts of kinetic energy are transferred to smaller scales which flattens the corresponding VSF.

These interpretations of the examples are verified by the entire time evolution of the clouds. Fig. 2a shows that the measured ζ cease with time as the clouds contract under the influence of self-gravity. This is evident as the density and boundness of the clouds increases with as, as well as further gas falls into them (Paper II).

However, one also sees peaks in the profiles of ζ that represent a temporary deviation from the global evolution of the clouds. The origin of these features can easily be traced back to the SNe occurring in the environment of the clouds. To visualise this better, we add marks to Fig. 2 that represent the times when the SNe explode and the periods of time when the clouds are heavily accreting gas. The data are taken from Paper II, where mean distances between the sites of SNe and the centres of the clouds can also be found. Considering that the SNe shock fronts move at speeds of 50–100 km s^{-1} through the ISM and with distances between 30–100 pc to the clouds, the shocks need around 1 Myr, on average, to reach the clouds. Thus, one cannot only relate the major gas accretion events of the clouds to the arrival
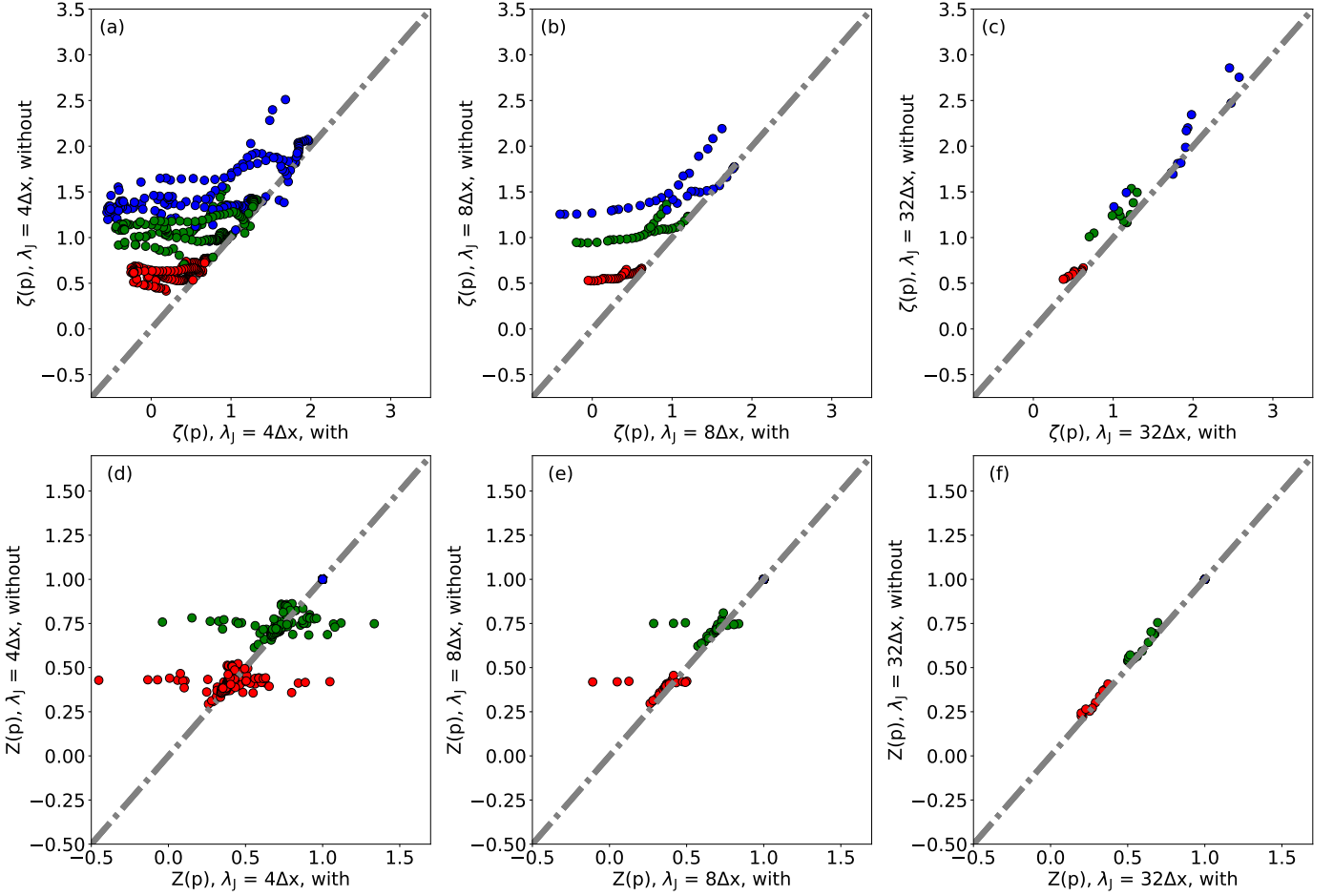
Figure 5: Comparison of ζ (*top*) and Z (*bottom*) measured based on density-weighted VSFs (*abscissas*) and non-weighted VSFs (*ordinates*).

of those SNe that indeed affect the evolution of the clouds, but also all significant variations in the evolution of ζ. In most of the cases, the SNe inject turbulent power into the systems which amplifies the VSFs at all scales, but in particular the large scales. The latter causes an elevation of ζ. Yet, the interaction between the clouds and the shocks lasts only for less than 0.6 Myr, after which ζ evolves back into the pre-shock conditions

The behaviour of M8 appears to contradict the explanations we have given for the evolution of turbulence within M3 and M4. However, looking at M8 in detail this is not the case. Paper II show in their Fig. 5 that M8 does not react as strongly to the onset of self-gravity as the other clouds do. For example, the mass of M8 remains almost constant for the first megayear while the other clouds strongly accrete gas from the ISM. Similarly, the velocity dispersion within M3 and M4 increases within the first 1.5 Myr while it is close to constant in M8 until the SN shock hits the cloud. Thus, we explain the evolution of ζ as follows: In the beginning, M8 evolves only slightly. It loses a small fraction of gas (Paper II, Fig. 5, *middle* panel). Therefore, the VSFs increase towards larger separations. At $t = 1.5$ Myr the shock front of the $t = 0.8$ Myr SN hits the cloud. That causes a short periods of extreme gravitational collapse, traced by the dip in ζ. As in the other clouds, the gas relaxes rapidly after the shock. However, the cloud continues to gravitationally contract in a more regular way. That is seen as slow decrease of ζ from $t = 1.8$ Myr on.

In summary, one can say that the scaling exponent, ζ, that is obtained by fitting a power-law relation onto the measured ve-

locity structure function, is a useful tool to understand and evaluate the time evolution of turbulence within molecular clouds. It is not only sensitive to both external (SNe) and internal (gravitational collapse) driving sources, but also reacts differently to the individual driving sources.

However, this diagnostic requires a series of time steps to be significant. According to She & Lévêque (1994) and Boldyrev (2002), $\zeta(3)$ is supposed to be equal or larger than unity whenever the gas experiences supersonic turbulence. Although this is definitely the case in the model clouds (Paper I; Paper II), one sees that $\zeta(3)$ declines far below 1 due to gravitational collapse. Thus, measuring ζ for individual moments in time, as observations would do, cannot fully describe the turbulence of molecular clouds.

The principle of "extended self-similarity" (Benzi et al. 1993, Sect. 2.2) offers a solution to this problem. The principle reflects the nature and the properties of intercloud turbulence, even when it is dominated by gravitational collapse. However, we also detect strong deviations that either reduce or increase the measured values of Z. Those derivations can be related to the physical forces that currently dominate the clouds.

We observe a similar behaviour in the time evolution of the self-similarity parameter $Z(p) = \zeta(p)/\zeta(3)$, shown in Fig. 3a. The peaks in the Z (for example, in M4 at $t = 4.1$ Myr) occur at the times when the scaling exponents of the VSFs, ζ, reach values close to or below 0. That means that the VSF becomes flat ($\zeta = 0$) or increases forward smaller scales ($\zeta < 0$). In this case,

9

self-gravitational contraction clearly dominates the cloud's evolution. It transfers the majority of turbulent power from the large to the small scales, where filaments and fragments are forming and accreting gas. The decrease in Z (for example, in M3 around $t = 1.8$ Myr), on the other hand, occur when SN shocks hit and heavily impact the clouds. This causes a sudden, but heavy increase of turbulent power on all scales, though on the larger scales more than on the smaller, resulting in a steepening of the VSF towards larger scales and an increase in ζ. The VSFs become more sensitive to the shock the higher their order is. Therefore, the $\zeta(3)$ increases more rapidly than $\zeta(2)$ and $\zeta(1)$, causing $Z(2)$ and $Z(1)$ to decrease.

In summary, Z is not as sensitive to gravitational contraction as ζ, although it is very sensitive to the inversion of scales that are dominant in turbulent power. It also traces the impact of SN shocks on the clouds. Whenever neither of these two extreme scenarios is acting on the clouds, the values of Z are close to the predicted values (see discussion below). This means that Z is, as ζ, a good tracer for the dominant forces driving the turbulence within the cloud, both internally and externally, as long as they are heavily impacting the cloud. The disadvantage is that one cannot use Z to distinguish between freely-floating fully-developed and moderate gravitational contraction, as one can do it with ζ. However, the advantage is that a single-epoch observation of Z is sufficient to trace extreme motions and driving sources within observed molecular clouds.

At the times when the clouds are not impacted by the above described extreme cases, one sees that the ratio of the VSF scaling exponents is mostly in agreement with predicted values for self-similar turbulence, although the clouds are dominated by gravitationally contracting motions during their evolution. The measured Z, thereby, do not uniquely follow the predictions of only Boldyrev (2002) or She & Lévêque (1994), but are normally between the predicted values of both theories. Recalling that both studies describe supersonic, fully developed turbulent flows, the only difference between them are the different geometries along which they allow the gas to flow. In the case of Boldyrev (2002), the gas flows are sheet-like, while they are filamentary in the work by She & Lévêque (1994).

Since M3 is heavily impacted by many SN shocks and heavy collapse motions, it does not allow us to make strong predictions about its 'steady-state' evolution. The other two clouds, on the contrary, are less externally impacted. This allows us to relate the developments of measured Z to the internal evolution of the clouds. In M8, Z follows the predictions by She & Lévêque (1994) for most of the cloud's evolution. This shows that M8 mostly transfers gas along filamentary substructures which means that the cloud is highly hierarchically structured already at the beginning of the simulations and before self-gravity is active. This also implies that the formation of filamentary structures does not require gravity (e.g., Federrath 2016). The fact that we do not detect fragments before the clouds have evolved under the influence of self-gravity for at least one megayear (see Paper III), however, demonstrates that gravity is essential for the fragmentation of filaments and formation of further substructures.

The evolution of Z in M4 shows a slightly different picture that still contains significant conclusion. While the values of Z in M8 are mostly constant over time, they decrease in M4, starting at values that are in agreement with the sheet-like flows of Boldyrev (2002) to those that are predicted for filamentary flows by She & Lévêque (1994). This demonstrates that M4 develops its hierarchical structure as it evolves under the influence of self-gravity. As a consequence, its turbulent structure becomes more

dominated by the filaments with time which causes the decline of $Z(p)$. Considering that the gas of M4 is indeed first flattened into more sheet-like geometry through the impact of the SNe (Ibáñez-Mejía et al. 2017) this observation is very interesting. It agrees with the studies, for example by Lin et al. (1965) or McKee & Ostriker (2007), that claim that molecular clouds are supposed to collapse in a dimension-losing, outside-in fashion that does not require any initial substructures within the clouds.

In summary, Z reflects the global geometry of turbulence within molecular clouds. Thereby, the measure values of Z are in good agreement with predictions from self-similarity theory, as long as one carefully ensures that the dominating turbulence mode in the cloud matches the modes that are considered in the respective theory. This makes Z a reliable parameter for examining turbulence modes in observational studies. Furthermore, the time evolution of Z shows how the geometry of turbulence is changed due to the gravitational contraction, e.g. from sheet-like to filamentary vortices, accompanies the change of basic parameters describing the turbulent structure of the entire cloud. Z can also deviate from the predicted values. This, however, only occurs in time spans of extreme turbulence driving, such as SN shocks. Fortunately, these extreme driving sources affect Z differently: SN shocks decrease Z, while gravity causes a quasi-momentary peak in Z. In both cases, Z relaxes to the pre-perturbation values within a short time.

4.1. Comparison to Line-of-Sight Velocities

In this paper, we do not only aim to analyse the mechanisms that drive turbulence within simulated molecular clouds, but also to provide a practical tool that can be used understand the dynamical processes within the observed ISM better. For the latter, it is necessary to examine its applicability under and the dependencies of the obtained results on all relevant conditions. As we have chosen to use VSFs for our analysis it is evident that we first need to investigate how the function reacts to the number of measured velocity vector components.

We recall that Equ. (1) gives the VSF as the mass-weighted average of relative velocities between the clouds' gas cells. This means that for a proper one needs all three components of the three-dimensional (3D) velocity vector for each contributing cell. Observations, however, normally measure only the one-dimensional (1D) component along the line-of-sight (los), also known as local standard of rest velocity. If the gas moves exclusively along the los both the 3D and 1D VSF will return the same results. If the gas is, contrary, driven into directions perpendicular to the los only the 1D VSF will be absolutely 0.

In this section, we discuss the results considering this aspect. Hence, we use the same data of the model clouds as before and produce three subsamples by projecting the 3D velocity vectors onto the three major axes x, y, and z, respectively. The derived ζ and Z for each subsample are shown in Figs. 2b and 3b.

In Sect. 3.1 we have seen that the ζ and Z derived from the 1D VSFs generally evolve similarly as those derived from the 3D VSFs. Yet, we have also seen that individual sight lines may evolve differently. Those differences are generated when the gas is significantly more driven into the corresponding sight lines than into the others (analogously to the simple scenario described above).

For example, for the first two megayears of the evolution of M4 the values of Z along the y axis are significantly higher than those observed along the other axes and the predicted values. Recalling that a higher value of Z correspond to an episode of very strong gravitational contraction, we can conclude that

within this time span M4 is dominantly collapsing along its y axis. The values of Z that are measured for the other two axes agree with this conclusion as they are best predicted by Boldyrev (2002) who describes a sheet-like turbulence. Note that this effect is only visible as we analyse the three dimensions separately, as the 3D VSFs (see Fig. 3) do not mirror the driving of the gas along the y axis at all.

In summary, we see that for a fully developed 3D turbulent field we expect that 1D VSFs behave similarly to 3D VSFs. However, when there is preferred direction along which the gas flows the 1D and 3D VSFs differ significantly from each other. Thus, it is predictable that observed VSFs can reflect the nature of turbulence within molecular clouds unless there is clear evidence that the gas is driven into a particular direction (e.g., by an HII region, or SN shock front).

Note, however, that in this analysis does not take typical los effects, such as optical depth effects or blending, into account. As we have seen in Sect. 3.3, a good knowledge of the velocity information is essential for a proper interpretation of the obtained VSFs. Future studies need to investigate this point in more detail by performing elaborated radiative transfer calculations.

4.2. The Effect of Jeans Length Refinement

In Sect. 3.2, we motive the need to investigate the influence of Jeans refinement on VSFs. In particular, we examine how the choice of using the minimally required refinement compares to a generally recommended refinement level, including the differences in total energy and resonances seen in the power spectra. To do this, we use the data by Paper II that resolve the Jeans length in M3 twice ($\lambda_J = 8\Delta x$) and eight times ($\lambda_J = 32\Delta x$) finer as the original simulations ($\lambda_J = 4\Delta x$).

In Fig. 4 we have seen that the choice of refinement level must not have a significant influence on the measurements and evolution of both ζ and Z. $\lambda_J = 4\Delta x$ and $\lambda_J = 8\Delta x$ are in very good agreement with each other. This means that, although refining Jeans lengths with 4 cells misses about 13% of kinetic energy, the effect on the structure and behaviour of the turbulence is rather small and not traced by a VSF analysis.

However, the bottom row of Fig. 4 also shows that such an agreement is not self-evident as $\lambda_J = 32\Delta x$ differs more from $\lambda_J = 4\Delta x$ the higher the order of the VSF is. Following the explanations in Sect. 3, the behaviour of ζ and Z in the $\lambda_J = 32\Delta x$ runs corresponds to the reaction of the cloud's gas to a shock wave running through the cloud; caused by a supernova that exploded before $t = 0$ Myr. Indeed one sees a SN at a distance of 172 pc at $t = -1.11$ Myr. Due to the distance the shock front is too weak to effectively compress the gas within M3. This is why it has not been detected previously in the less refined samples. However, the SN explodes far below the mid-plane of the modelled disk galaxy, in a region without dense gas. This means that the shock wave that has been injected by the explosion is less damned as it propagates through the ISM. By the time the front arrives at M3 it is still energetic enough to drive strong winds, with velocity above 300 km s^{-1}, at the closer edge of the cloud. This causes an increase of VSFs at longer lag scales and the increase of ζ, as well as the drop in Z.

Thus, derivations of measured Z to predicted values do only trace external turbulent driving. Whether the source is a SN shock front propagating through the cloud or a strong wind, cannot be distinguished by Z only. Yet, Z remains a fine probe for the geometry of turbulence and the scales at which turbulence is driven.

4.3. The Effect of Density Thresholds

In Sect. 3.3 we test the influence of the density threshold that defines the volume of our interest on the evolution of VSFs. In this particular case, we normally define our clouds as volumes of connected gas cells with densities above a certain value $n_{cloud} = 100$ cm^{-3} Paper I; Paper II. Although this approach is in agreement with typical post-processing methods of observational data, by doing so we only work with ≤1.5% of the cubes' volumes.

As the post-processing of the entire data cubes, which would be result when removing the density threshold and setting $n_{cloud} = 0$ cm^{-3}, would be too computational expensive, we have decided to reduce the number of considered radomly chosen cells to 5% of the total number of cells. We emphasise again that this does not mean that we only calculate the relative velocities between those 5% of cells. Rather this subsample of cells represent the starting vectors x to which the velocities of all other cells $x + \ell$ in the same cube are compared to. This way we reduce the risk of ignoring or emphasising any spatial direction or angle.

Further note that by choosing the starting points randomly we ensure that all parts of the cubes are considered. As a consequence, there is only a verys little likelihood (5% × 1.5% = 0.075%) that cells that are associated with the clouds are chosen. Therefore, we emphasise that it is very likely that the two subsamples (no density threshold and cloud-only) do not necessarily have a common set of starting vectors. Yet, as we here still calculate relative velocities to all other cells in the cube, and that includes all cells making up the clouds, the resulting VSFs of the $n_{cloud} = 0$ cm^{-3} sample also consists of most of the information of the inner-cloud interactions.

In Sect. 3.3 we see that the structure and evolution of VSFs strongly depends on whether or not there is a density threshold. In the previous case, where $n_{cloud} = 100$ cm^{-3}, we have seen a mostly straight decline of ζ and a rather, but not completely constant evolution of Z over time that reflect the conteraction of the clouds due to self-gravity. Here, in the $n_{cloud} = 0$ cm^{-3} sample, however, we see a completly different picture. There is still a slightly declining trend in ζ. Yet, the evolutions are dominated by random fluctuations.

We also see that the measured Z evolves even more constantly than what we have seen in the previous scenarios. This is true for the entire time range and the exactly same values of Z measured for all clouds. Therefore, the source that drives the turbulence on the scales of the modelled ISM is constantly and isotropically acting on the diffuse gas. This means that we here study the ISM that fills the entire modelled galaxy, not only the closer environment of all clouds. Thus, the ISM matter around the clouds is constantly highly driven by different sources and individual events, like a single SN, do not have as a high impact on the state of turbulence of the ISM as on the gas within the clouds which is comparably quite.

We conclude that the decision whether or not a density threshold is used for ascertaining insights on the turbulent composition of the observed gas has a significant and direct influence on the resulting VSFs. As mentioned previously, applying a density threshold is often unavoidable as it is a straight-forward approach to filter the data on the actual area of interest. In observational studies it is even always present as minimal collision rates for excitation or the sensitivity of detectors automatically result in implicit intensity and density thresholds. Although we have only tested two specific setups in this context we have seen the significance of a proper choice of the density threshold, as

well as a proper discussion of the obtained results considering the used threshold as one of the defining parameters.

4.4. The Effect of Density Weighting

In this subsection, we discuss the effect the ambiguous definition of VSFs has on the measurements. With this we mean that the VSF can be computed with or without taking density weighting into account. This ambiguity originates in the type of data one analyses. In general, the VSF considers the average relative velocity between each two Lagrangian particles. As each fluid particle stores its complete set of information its mass, and therefore its inertia, is automatically considered when iterating its velocity; and Eq. (8) is sufficient to derive the VSF of the fluid properly. In our case, however, we examine Eulerian data that store the parameter of the fluid on a static grid. The information of individual particles and vortices are thereby averaged over the grid. Consequently, it is important to consider this when computing the VSF; which is done by using the density-weighted definition of the VSF given in Eq. (1).

Although the motivation why the different definitions exist and are used for non-overlapping samples of data, it is not yet clear how the results obtained with the two approaches relate to each other. This we do by applying both ansatzes on our data. The results are presented in Sect. 3.4. There we see considering the density weighting or not does not have a significant effect on the data, but only as long as the turbulence is dominated by the large scales. However, as the clouds evolve the differences increase because the non-weighted VSFs never drop below 0.5. This is because the non-weighted VSF treats all cells equally, no matter whether they represent a volume element of the clouds or one of the ISM, while the weighted VSF gives more weight to the matter within the clouds. As long as the turbulence is dominated by large scales this does not cause a notable difference as these long separations, considering the density threshold, represent cells on the outer surface of the clouds, with similar densities and conditions. The small lag scales, contrary, reflect how the conditions change within the clouds, with density gradients becoming larger towards the centre of the clouds and increasing faster than the relative velocities of neighbouring cells. Here, the density weighting becomes crucial to compensate for the fact that the higher density represents a higher number of particles in a Lagrangian framework. However, if one does not consider this (as we have done in Sect. 3.4) the inner regions of the clouds are not processed correctly. This ends in a situation where the large scales never seem to loose their dominance, and ζ never becomes close or less than 0; a situation that does not reflect the reality.

Nevertheless, Fig. 3e illustrates that these differences can only be traced by ζ alone. Besides the features created when ζ becomes close to 0 in the density-weighted VSFs, the measured Z have similar values, evolve and reacts to external driving mechanisms similarly independently based on which approach they are computed. This observation is true for all Jeans refinement levels, as Fig. 5 demonstrates.

We conclude that deriving the VSF from smooth density distributions without considering density weighting does not affect the behaviour of ζ and Z, as long as the turbulence is dominated by large scale vortices, while it has a significant effect on the measurements when the small scales become dominant. The latter is particularly important as this finding directly influences the conclusions one may draw on the scales and mechanisms that drive the turbulence based on the measured ζ. Not only does ζ become insensitive from the influence of gravitational con-

traction with time, the non-weighted VSFs do also not reflect when the majority of kinetic energy has been transferred to small scales. Thus, it is highly important to clarify which definition of VSF is used and if it is indeed suitable for the respective study. Yet, our analysis also shows that the principle of self-similarity relativises the deviations between the two approaches as the different orders of the VSFs keep scaling in the same way.

5. Summary & Conclusions

In this paper, we analyse the turbulent structures of molecular clouds and filaments that have formed within 3D AMR FLASH simulations of the self-gravitating, magnetised, supernova-driven ISM by Ibáñez-Mejía et al. (2016). The main results are as follows.

- The scaling of velocity structure functions (VSFs) is sensitive to both internal (gravitational contraction) and external (SN shocks, winds) driving sources of turbulence. Applied on simulated data, the time evolution of the scaling exponent, ζ, can reveal which driving mechanism dominates the turbulence of an entire molecular cloud. The self-similarity parameter, Z, though, is not directly sensitive to gravitational contraction. Yet, it can be used as observational tracer as it significantly reacts to SNe and winds.
- As long as the molecular cloud is not affected by a shock, Z is in good agreement with predicted values for supersonic flows. This makes it a fine probe for the properties of dominant turbulent modes, such as the geometry, and their evolution in the context with the evolution of the cloud.
- We test the influence of Jeans refinement on the VSFs. We find that the absolute amount of kinetic energy does not influence the evolution of ζ and Z, as long as the power spectrum is properly resembled, or similarly resembled by the compared samples.
- We see that the behaviour of the VSFs can be tracked with similar results based on 3D (i.e., from simulated data) and 1D (i.e., from observational data) velocity information, as long as there is no dominating flow driving the gas into a direction perpendicular to the line of sight. In the general case of a fully developed turbulent field, the both ζ and Z evolve similarly in both scenarios, even though the actual values might not be similar.
- We test the influence of introducing a density threshold on the VSFs. We see significant differences both quantitatively and qualitatively. The VSFs that based on the unfiltered data are much steeper than the cloud-only VSFs and do not reflect any interaction with any of the driving sources, including SN shocks. The measured Z values are constant in time and and for all clouds. This means that the turbulence we examine in this sub-project reflects the ISM in our entire galactic-scale simulations. The values of Z are slightly below the value predicted for a filamentary flow by **?**. We conclude that the turbulence in the modelled ISM consists of vortices that are similar to filamentary flows, yet with a ratio of average length scale of the two moments being more equal to unity than in the filamentary case.
- We investigate the influence of defining the velocity structure function with and without taking density weighting into account. We see that the general, qualitative behaviour is traced by both ansatzes in the same way. In the case of the non-weighted VSF the scaling exponents are always positive and evolve flatter than they do for the density-weighted VSF.

Our analysis shows that VSFs are fine tools for examining the driving source of turbulence within molecular clouds. Therefore, we recommend its usage in future studies of molecular clouds. However, studies that utilise VSFs need to precisely review the assumptions and parameters they imply in their analysis as those can have a significant influence on the out-coming results.

For the model clouds, the VSFs illustrate that gravitational contraction dominates the evolution of the clouds for most their evolution, with short periods within which SN shock waves accelerate the turbulent powers on all scales. Yet it requires further studies to verify this to be the common fragment formation scenario. Especially, a higher Jeans length refinement is needed to resolve the velocity structures on scales of individual grid cells (0.1 pc in this case). This is crucial for following the local behaviour of the gas as neither the average behaviour of the filaments nor the dominant turbulence driving source of the entire molecular clouds mirror the underling flow patterns that are necessary for this scenario.

References

Ballesteros-Paredes, J., Hartmann, L. W., Vázquez-Semadeni, E., Heitsch, F., & Zamora-Avilés, M. A. 2011a, Monthly Notices Roy. Astron. Soc. , 411, 65

Ballesteros-Paredes, J., Vázquez-Semadeni, E., Gazol, A., et al. 2011b, Monthly Notices Roy. Astron. Soc. , 416, 1436

Banerjee, S. & Galtier, S. 2013, Phys. Rev. E., 87, 013019

Benzi, R., Biferale, L., Fisher, R., Lamb, D. Q., & Toschi, F. 2010, Journal of Fluid Mechanics, 653, 221

Benzi, R., Ciliberto, S., Tripiccione, R., et al. 1993, PhysRevE, 48, R29

Boldyrev, S. 2002, Astrophys. J. , 569, 841

Boneberg, D. M., Dale, J. E., Girichidis, P., & Ercolano, B. 2015, Monthly Notices Roy. Astron. Soc. , 447, 1341

Brunt, C. M. & Heyer, M. H. 2013, Monthly Notices Roy. Astron. Soc. , 433, 117

Brunt, C. M., Heyer, M. H., & Mac Low, M.-M. 2009, Astron. Astrophys. , 504, 883

Burkhart, B., Collins, D. C., & Lazarian, A. 2015, Astrophys. J. , 808, 48

Chira, R.-A., Kainulainen, J., Ibàñez-Mejía, J. C., Henning, T., & Mac Low, M.-M. 2017, ArXiv e-prints

Dekel, A. & Krumholz, M. R. 2013, Monthly Notices Roy. Astron. Soc. , 432, 455

Federrath, C. 2016, Monthly Notices Roy. Astron. Soc. , 457, 375

Fleck, Jr., R. C. 1980, Astrophys. J. , 242, 1019

Fryxell, B., Olson, K., Ricker, P., et al. 2000, Astrophys. J. Suppl., 131, 273

Galtier, S. & Banerjee, S. 2011, Physical Review Letters, 107, 134501

Gotoh, T., Fukayama, D., & Nakano, T. 2002, Physics of Fluids, 14, 1065

Hartmann, L., Ballesteros-Paredes, J., & Heitsch, F. 2012, Monthly Notices Roy. Astron. Soc. , 420, 1457

Heyer, M. H. & Brunt, C. M. 2004, Astrophys. J. Lett. , 615, L45

Ibáñez-Mejía, J. C., Mac Low, M.-M., Klessen, R. S., & Baczynski, C. 2016, Astrophys. J. , 824, 41

Ibáñez-Mejía, J. C., Mac Low, M.-M., Klessen, R. S., & Baczynski, C. 2017, Astrophys. J. , 850, 62

Kolmogorov, A. 1941, Akademiia Nauk SSSR Doklady, 30, 301

Krumholz, M. R., Bate, M. R., Arce, H. G., et al. 2014, Protostars and Planets VI, 243

Lin, C. C., Mestel, L., & Shu, F. H. 1965, Astrophys. J. , 142, 1431

Mac Low, M.-M. 2003, in Lecture Notes in Physics, Berlin Springer Verlag, Vol. 614, Turbulence and Magnetic Fields in Astrophysics, ed. E. Falgarone & T. Passot, 182–212

Mac Low, M.-M. & Klessen, R. S. 2004, Reviews of Modern Physics, 76, 125

McKee, C. F. & Ostriker, E. C. 2007, Ann. Rev. Astron. Astrophys. , 45, 565

McKee, C. F. & Zweibel, E. G. 1992, Astrophys. J. , 399, 551

Miyamoto, Y., Nakai, N., & Kuno, N. 2014, PASJ, 66, 36

Padoan, P., Pan, L., Haugbølle, T., & Nordlund, Å. 2016, Astrophys. J. , 822, 11

Schmidt, W., Federrath, C., & Klessen, R. 2008, Physical Review Letters, 101, 194505

Seifried, D., Walch, S., Girichidis, P., et al. 2017, ArXiv e-prints

She, Z.-S. & Lévêque, E. 1994, Physical Review Letters, 72, 336

Tan, J. C., Shaske, S. N., & Van Loo, S. 2013, in IAU Symposium, Vol. 292, Molecular Gas, Dust, and Star Formation in Galaxies, ed. T. Wong & J. Ott, 19–28

Truelove, J. K., Klein, R. I., McKee, C. F., et al. 1998, Astrophys. J. , 495, 821

Turk, M. J., Oishi, J. S., Abel, T., & Bryan, G. L. 2012, Astrophys. J. , 745, 154